Surface & Coatings Technology 483 (2024) 130750

Contents lists available at ScienceDirect

Surface & Coatings Technology

journal homepage: www.elsevier.com/locate/surfcoat

Tribological study of W-S-(C) sputtered coatings sliding against aluminium at elevated temperatures

Todor Vuchkov [a,b,*], Saniat Jahan Sunny [a], Albano Cavaleiro [a,b]

[a] Department of Mechanical Engineering, CEMMPRE, ARISE, University of Coimbra, Rua Luis Reis Santos, 3030-788 Coimbra, Portugal
[b] IPN - LED & MAT - Instituto Pedro Nunes, Laboratory for Wear, Testing and Materials, Rua Pedro Nunes, 3030-199 Coimbra, Portugal

ARTICLE INFO

Keywords:
Magnetron sputtering
Transition metal dichalcogenides
Self-lubricant
Tribology

ABSTRACT

Aluminium metal forming is often performed at elevated temperatures which can cause significant galling, damage to the produced parts and increased manufacturing costs. Self-lubricating thin films deposited by magnetron sputtering are good candidates for alleviating this issue. In this study we deposited three types of films containing transition metal dichalcogenides, of which one consisted only of WS_x and two films were alloyed with carbon. The aim of the work was to assess the ability of these coatings to reduce galling in sliding contacts with aluminium at elevated temperatures. The thermal analysis indicated that the maximum operating temperature should be ~400–430 °C, for the pure WS coating, and a higher value of ~480–490 for the carbon alloyed films. The coatings managed to provide friction reduction in all the testing conditions, except for the carbon alloyed one with the highest amount of carbon which could not provide lubrication against aluminium at 400 °C.

1. Introduction

Aluminium-alloys are ever more increasingly used in the automotive industry due to their good stiffness-to-weight ratio, enabling significant reduction in energy consumption and CO_2 emissions. One issue with the usage of aluminium alloys is the difficulty on their manufacturing, in particular by forming processes. At room temperature they have poor formability and suffer springback. Therefore, they are often formed at elevated temperatures (up to 500 °C). Forming aluminium at elevated temperatures generates tribologically related issues, namely they tend to cause adhesive wear and galling, i.e. there is material transfer from the workpiece to the die/tool. Severe galling results in significant damage to the produced part, raising the manufacturing and tool maintenance costs as well as increasing the energy consumption.

Reducing the adhesive/wear galling is typically through the use of lubricants. Considering the elevated temperatures used (350–450 °C), the effectiveness of conventional liquid lubricants is impeded, and solid lubricants can be, therefore, a good option. Self-lubricating coatings deposited by physical vapour deposition are reported for contacts involving sliding against aluminium [1]. In this work, the authors tested hydrogen-free diamond-like carbon (DLC) coatings against 319 Al alloy at temperatures ranging from RT to 300 °C. They observed an increase in the coefficient of friction with temperature, with a value up to 0.6–0.7 during the tests at 300 °C. It should be noted that the coating was completely worn during testing at 300 °C followed by severe material transfer from the counterbody to the exposed tool steel. B_4C and hydrogenated DLC coatings were also tribologically tested against aluminium at elevated temperatures [2]. B_4C did not provide friction reduction due to the adhesion of aluminium towards the coating. On the other hand, the hydrogenated DLC coating managed to provide friction reduction until 200 °C, by establishing hydrogen terminated carbon-based tribofilms. At temperatures over 200 °C the hydrogenated DLC showed a significant increase in wear. Elevated temperature testing of aluminium against tool steel without any added lubricant was also reported in [3]. They reported an increased mass loss of the aluminium counterbodies at temperatures between 150 and 250 °C. Moreover, the formation of metal oxide tribolayers at the highest temperatures of 350 and 450 °C was also reported which stabilized the COF and limited the wear. Nevertheless, the COF during testing in this temperatures range was up to 1–1.2. Self-lubricating Ni-based laser claddings for friction reduction in contacts involving aluminium at elevated temperatures were studied by Torres et al. [4]. The authors tested the claddings against the aluminium alloy 6082 at a temperature of 300 °C. They observed friction reduction when the claddings contained Ag and MoS_2 as a solid lubricant. The friction reduction was the result of the formation of either silver or nickel-sulfide tribofilms. A combination of self-

* Corresponding author at: Department of Mechanical Engineering, CEMMPRE, ARISE, University of Coimbra, Rua Luis Reis Santos, 3030-788 Coimbra, Portugal.
E-mail address: todor.vuchkov@ipn.pt (T. Vuchkov).

https://doi.org/10.1016/j.surfcoat.2024.130750
Received 3 November 2023; Received in revised form 28 March 2024; Accepted 2 April 2024
Available online 4 April 2024

Table 1
Chemical composition and thickness of the deposited coatings.

Coating	Elemental composition (at. %)				S/W ratio	Total thickness (μm)
	C	S	O	W		
WS	6.7 ± 0.1	51.2 ± 0.3	8.8 ± 0.1	33.5 ± 0.3	1.53	1.39
WSC1010	27.6 ± 0.2	39.3 ± 0.1	4 ± 0.1	29.2 ± 0.1	1.35	1.42
WSC1016	35.5 ± 0.1	36.3 ± 0.1	3 ± 0.1	25.3 ± 0.1	1.43	1.41

lubricating coatings with the addition of lubricants like graphene, hexagonal boron nitride and graphite is also considered for elevated temperature sliding against aluminium [5]. The main achieved results were the significant friction reduction when graphene additives were utilized with both uncoated and coated tool.

In summary, for contacts involving sliding against aluminium, the available literature provides information mainly regarding the usage of carbon-based materials as thin films/coatings (e.g. DLC coatings) or other coatings containing transition metal dichalcogenides (TMD - such as MoS_2) and/or soft metals (such as Ag) as additives. Therefore, a potential solution for contacts involving sliding against aluminium at elevated temperatures would be carbon-alloyed TMD thin films. These coatings are often deposited by magnetron sputtering [6]. They usually have a nanocomposite structure consisting of an amorphous carbon matrix with TMD crystals embedded in it. This structure is beneficial as it overcomes the disadvantages of the TMD materials (e.g. their low hardness) without hindering their lubricity. The amorphous-carbon matrix can also provide lubricity through the formation of graphite-like tribofilms. The transition metal dichalcogenides are solid lubricants that work well in inert or low humidity-containing environments [7]. They have low shear strength due to their layered crystal structure consisting of a transition metal sheet of atoms sandwiched between two sheets of chalcogen atoms. The bonding within this structure is covalent and it forms a TMD layer. The TMD crystals consist of many of these layers bonded together with weak van-der-Waals forces creating a mechanical weakness. Under shear stresses, the layers slide easily due to the weak bonding and if they are present at a sliding interface they can provide lubrication. Within this group of compounds, WS_2 is quite promising for applications involving operation at elevated temperatures. This is due to its higher oxidation temperature, which can go up to 480 °C, compared to ~370 °C reported for MoS_2 [8]. In our previous work [9], a carbon alloyed TMD coating was tested at elevated temperatures up to 400 °C against steel. A very low coefficient of friction (down to ~0.01) was observed. The very low friction behavior at elevated temperatures was attributed to the presence of TMD-based tribofilms which have low shear strength in environments that lack humidity.

In this work, we report the synthesis of WS_2 containing coatings (WS_x and W-S-C) by magnetron sputtering for potential application in contacts involving sliding against aluminium at elevated temperatures. This work aims at assessing the ability of WS_2 containing sputtered at reducing friction and wear in contacts with aluminium at elevated temperatures, relevant for forming applications. Three coatings with different carbon content below ~35 at. % were prepared.

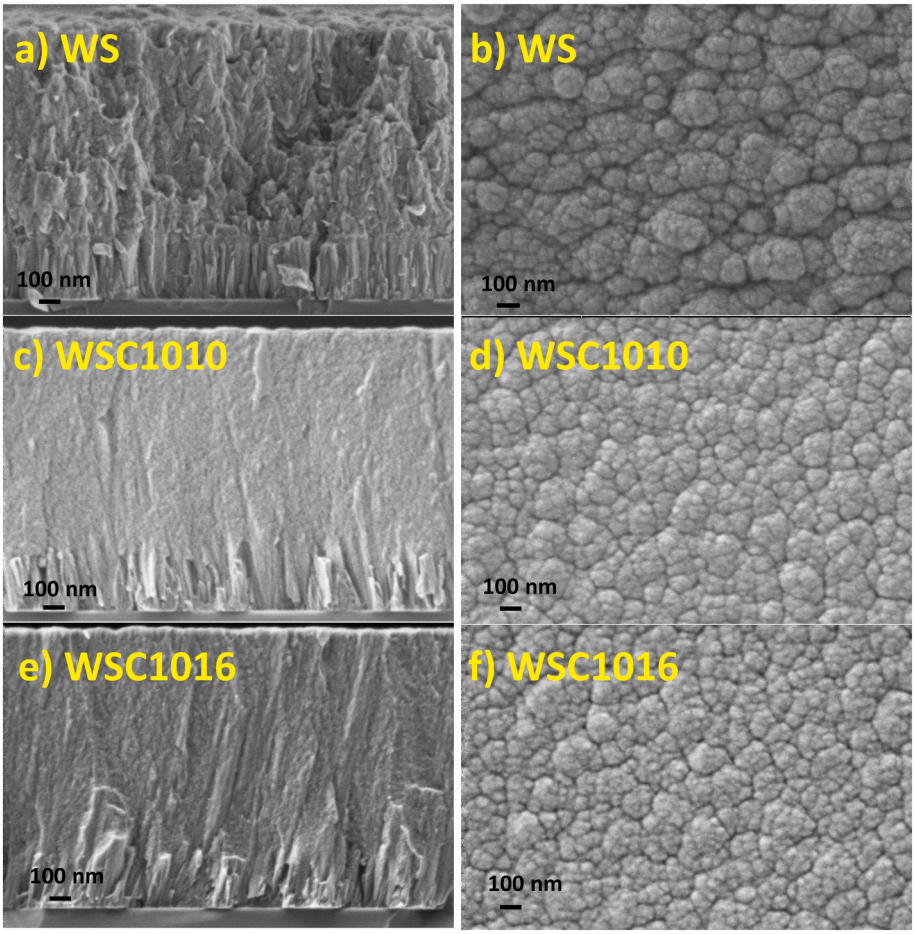

Fig. 1. Cross sectional and top-surface morphology of: a,b) WS; c,d) WSC1010 and e,f) WSC1016.

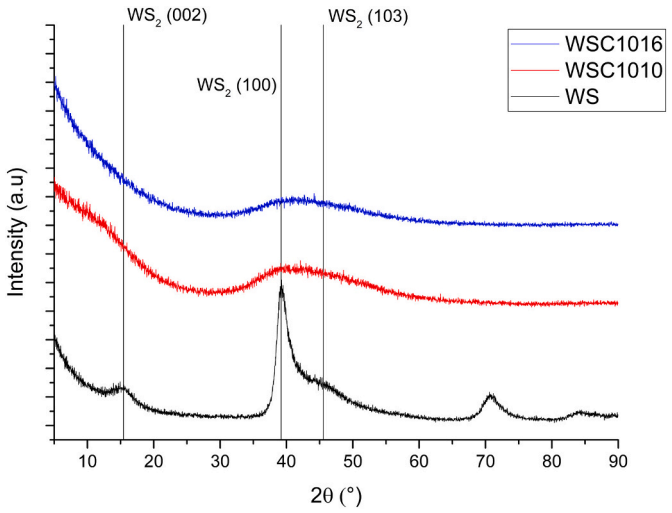

Fig. 2. X-ray diffractograms.

2. Experimental methods

2.1. Coating deposition

The W-S-(C) coatings were deposited by closed-field unbalanced magnetron sputtering using a Teer UDP 650/4 equipment. A schematic of the target and substrates configuration can be seen in our previous publication [10]. The chamber was equipped with 4 targets of which one was WS_2, 2 were graphite and one was Cr. The substrates used were plates made of AISI H11 tool steel with a length of 30 mm, width of 15 mm and thickness of 4 mm. The tool steel had a hardness of ~560 HV1, and since during the coating process the temperatures are below 200 °C, we do not expect any changes in its hardness after coating. Additionally, Si wafers were also coated. The films were also deposited on polished FeCrAl substrates, for high temperature X-ray diffraction, and alumina (Al_2O_3) substrates, for thermo-gravimetric analysis. Before deposition the steel substrates were mirror-like polished with SiC papers and diamond suspension (down to 1 μm particle size), reaching an average surface roughness of $R_a < 20$ nm. Before placing in the chamber, they were ultrasonically cleaned in acetone and ethanol for 15 min each and dried with warm air. They were placed on a holder in the middle of the chamber at a distance of 25 cm from the targets. A base pressure $< 10^{-3}$ Pa was reached before starting the deposition. The coatings were deposited at ~0.4 Pa in an Ar atmosphere. Before the deposition the targets were sputter cleaned in pairs for 20 min each using a DC power of 1000 W (Advanced Energy Pinnacle). The substrates were simultaneously sputter cleaned for 40 min using pulsed-DC power (Advanced Energy Pinnacle Plus), in voltage-mode, with 600 V, a frequency of 250 kHz and a reverse time of 1.6 μs. A Cr interlayer was deposited by sputtering the Cr target for 10 min with a power of 2000 W. Afterwards a gradient layer was deposited by ramping down the power used on the Cr target to 0 W and ramping up the power used for the W-S-C coatings. Three different coatings were deposited based on the experience accumulated during last years with this system (see e.g. [9–12]). The carbon-alloyed coatings were chosen to have low to moderate carbon contents in order to have relatively high contents of lubricious WS_2 while attaining moderate hardness which should positively affect the wear resistance. A pure WS_x coating (WS) was deposited by sputtering only the WS_2 target using 1000 W of power. In this coating a negative substrate bias of 50 V (pulsed DC, with 0.5 μs reverse time and 250 kHz frequency) was used. The two W-S-C coatings were deposited by keeping the power used on the WS_2 target at 1000 W and varying the power applied on the graphite targets. The power applied on the graphite targets was 500 W on each one (1000 W total) for the coating WSC 1010 and 800 W on each (1600 W total) for WSC 1016. No negative substrate bias was used for the coatings containing carbon. No intentional substrate heating was used. The total deposition time was 120 min, including 10 min for interlayer deposition and 10 min for gradient layer deposition.

2.2. Morphological and structural characterization

The morphology of the coatings was analyzed by field-emission scanning electron microscopy (FESEM, Zeiss Merlin). Top-surface and cross-sectional imaging was performed on coatings deposited on Si wafers. Imaging was acquired in secondary electron mode with an accelerating voltage of 2 kV. The composition was analyzed by wavelength dispersive spectroscopy (WDS) with a detector attached to the FESEM. The accelerating voltage used for the analysis was 15 kV.

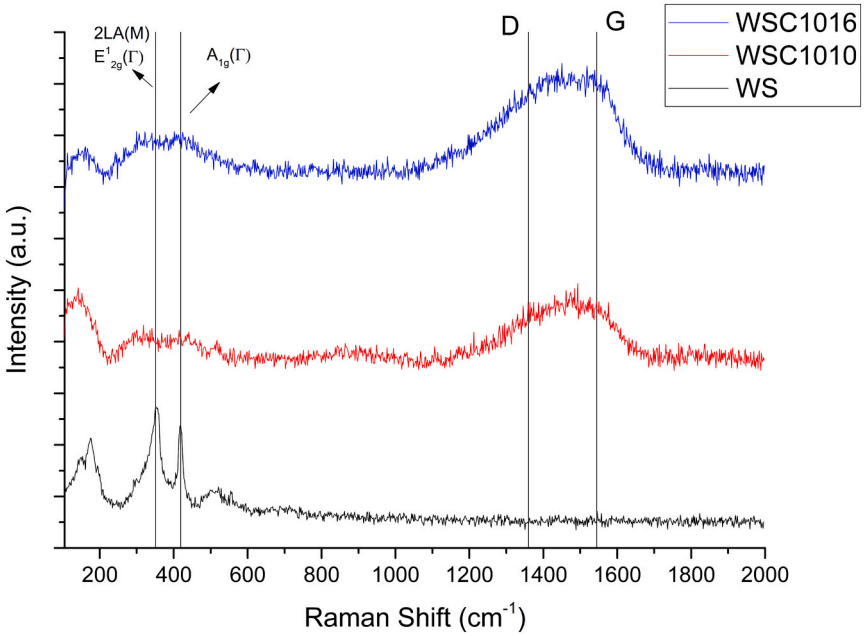

Fig. 3. Raman spectra of the deposited coatings.

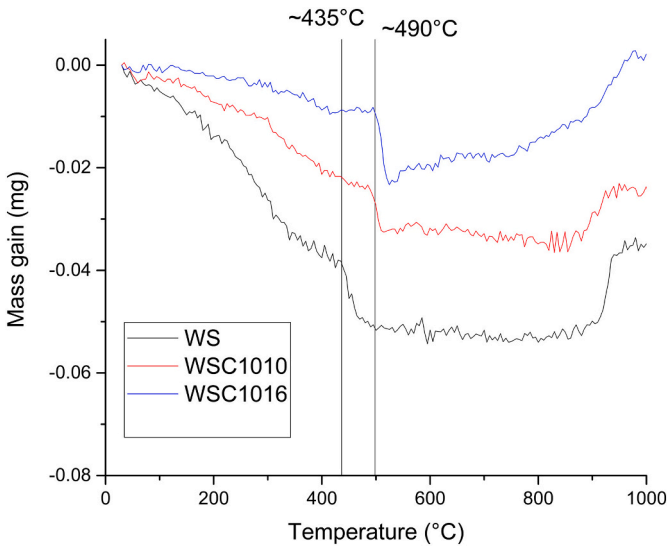

Fig. 4. Results from the TGA experiments.

Grazing incidence X-ray diffraction (GIXRD) was performed using a Phillips X-pert Pro MRD. A cobalt X-ray source was used ($\lambda = 1.79$ Å) in the angle range of $2\theta = 5$–$90°$. The incidence angle was fixed at 2°.

Raman spectroscopy was performed using a Renishaw InVia™ Raman microscope. A 50 mW diode laser with a wavelength of 532 nm was utilized. The power of the laser was reduced, using ND filters, to 0.1 % and 0.5 % for the WS and the WSC coatings, respectively. A 100× objective was used. The exposure time was set to 10 s with 5 accumulations (total time 50 s). This value allowed for Raman analysis of the samples without any structural transformations (graphitization and oxidation) due to excessive heating.

2.3. Thermal analysis

Thermogravimetric analysis (TGA) was performed using films deposited on Al_2O_3 substrates. The films were heated to temperatures up to 1100 °C using a NETZSCH TG 209F1 Libra instrument. The heating rate was 10 °C/min. During the test the films were exposed to synthetic air. As a reference uncoated substrate was also tested and these results were used for the baseline removal. Additionally, in-situ high temperature GIXRD was performed in ambient conditions using a high temperature stage. The X-ray source and the acquisition parameters were the same as explained in the previous section. The selected temperatures were 200 °C, 400 °C and 500 °C.

2.4. Mechanical and tribological characterization

The hardness and reduced modulus were measured by nanoindentation using a Micromaterials Nanotest Vantage system, utilizing a Berkovich-type indenter. Indentation was performed with 6 loads in the range of 0.5–3 mN, with 9 indentation per load. The data was processed by the methods proposed by Oliver and Pharr [13]. The reduced

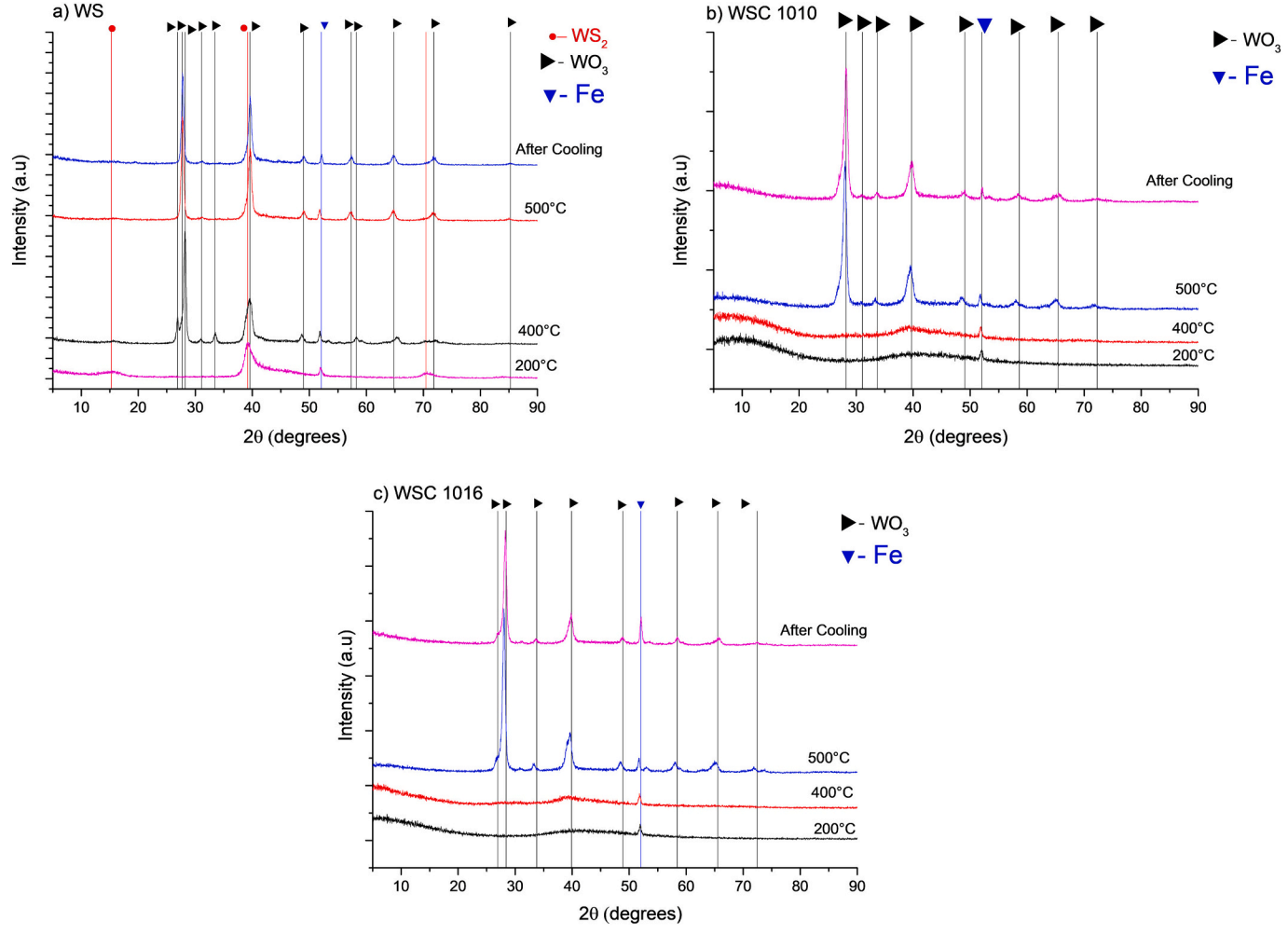

Fig. 5. In-situ high temperature X-ray diffraction results.

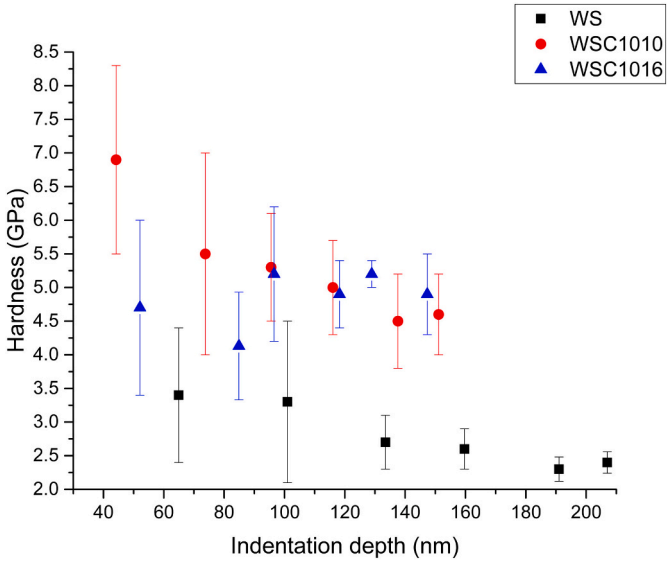

Fig. 6. Hardness of the coatings as a function of indentation depth.

Table 2
Critical loads obtained from the scratch testing experiments.

Coating	Critical Load (N)		
	Lc_1	Lc_2	Lc_3
WS	–	19 ± 1	>70
WSC1010	5 ± 1	27 ± 1	>70
WSC1016	6 ± 1	26 ± 1	>70

modulus was assessed following the ISO 14577-4 standard [14]. Namely, the measured reduced modulus was plotted against the normalized contact radius (a/t), where a is the contact radius and t is the thickness of the coating. The reduced modulus of the coating was then obtained by extrapolating the value to zero penetration depth.

The adhesion of the coatings was analyzed with scratch testing following the ISO 20502:2005 standard [15]. A Rockwell C conical indenter with a radius of 0.2 mm was used. The load was set between 2 and 70 N. The load rate was set at 10 N/mm with a sliding rate of 10 mm/min. The experiments were performed on an Rtec MFT 5000 multifunctional tribometer.

The tribological testing was performed in reciprocating pin-on-plate configuration using a module attached to the Rtec MFT 5000 tribometer. The counterbodies were 10 mm diameter aluminium balls (Aluminium 1050), with a hardness of ~30 HV. Spherical counterbodies were used since in flat pin on flat configurations issues with edge effects were observed. The load was 5 N, resulting in an initial maximum contact stress of ~0.8 GPa at room temperature. Three testing temperature were used, room temperature (RT), 200 °C and 400 °C. The RT testing was performed in lab conditions with a temperature of 24 ± 1 °C and a relative humidity (RH) of 40–55 %. The reciprocating frequency and the stroke length were 5 Hz and 6 mm, respectively, resulting in an average sliding speed of 0.06 m/s. The test duration was 500 s with a total number of cycles of 5000. For a better simulation of a hot forming process other configurations for tribological testing are typically used like the crossed-cylinder/load scanning test, where fresh surfaces are in contact during a load increase [5]. We decided to perform a simpler, reciprocating ball-on-flat test for a faster screening of the studied coatings since there is a lack of information in the literature about their performance in contact with aluminium at elevated temperatures. Furthermore, there is generally more data from ball-on-flat testing which facilitates the comparison of the performed worked with the literature available. The analysis of the spherical counterbodies after testing was performed with an Alicona Infinite Focus 3D profilometer. The coating wear tracks were analyzed by white light interferometry (WLI, Rtec Sigma). The wear volumes of the coatings were calculated from the 3D data and subsequently the wear rate was calculated ($W_r = V/Fs$), where Wr is the wear rate (mm^3/Nm), V is the wear volume (mm^3), F is the normal load (N) and s is the total sliding distance in meters. The wear volume was calculated by extracting three cross-sectional profiles and multiplying it with the sliding distance, following the ASTM D7755-11 standard. In some of the wear tracks, there were sporadic zones that contained material transfer from the aluminium counter body, and in those cases, extraction of profiles was performed from the more homogeneous zones of the track. In the case of the tracks which contained only material transfer, no calculations were made.

3. Results and discussion

3.1. Composition, morphological and structural analysis

The chemical composition of the coatings, obtained by WDS and the total thickness (including a Cr interlayer of ~300 nm) are shown in Table 1. The WS coating showed slightly higher oxygen contents than the other coatings, which is expected due to its more porous morphology. The S/W ratio measured was ~1.53. The S/W ratio is lower than the stoichiometric one (2) due to the preferential resputtering of the S atoms caused by the bombardment with energetic species and the difference in the scattering behavior of S and W atoms, which have significantly different atomic masses. It should be noted that a WS

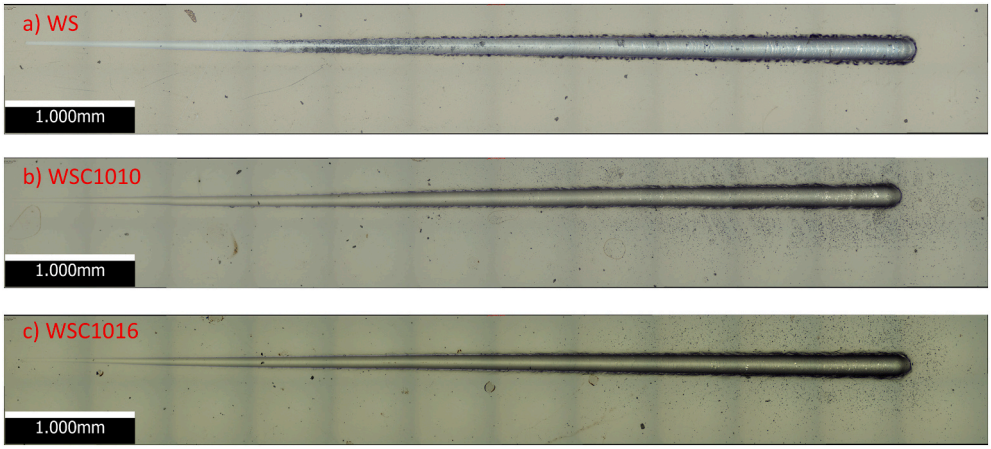

Fig. 7. Optical microgrpahs of the scratch tracks: a) WS b) WSC1010 c) WSC 1016.

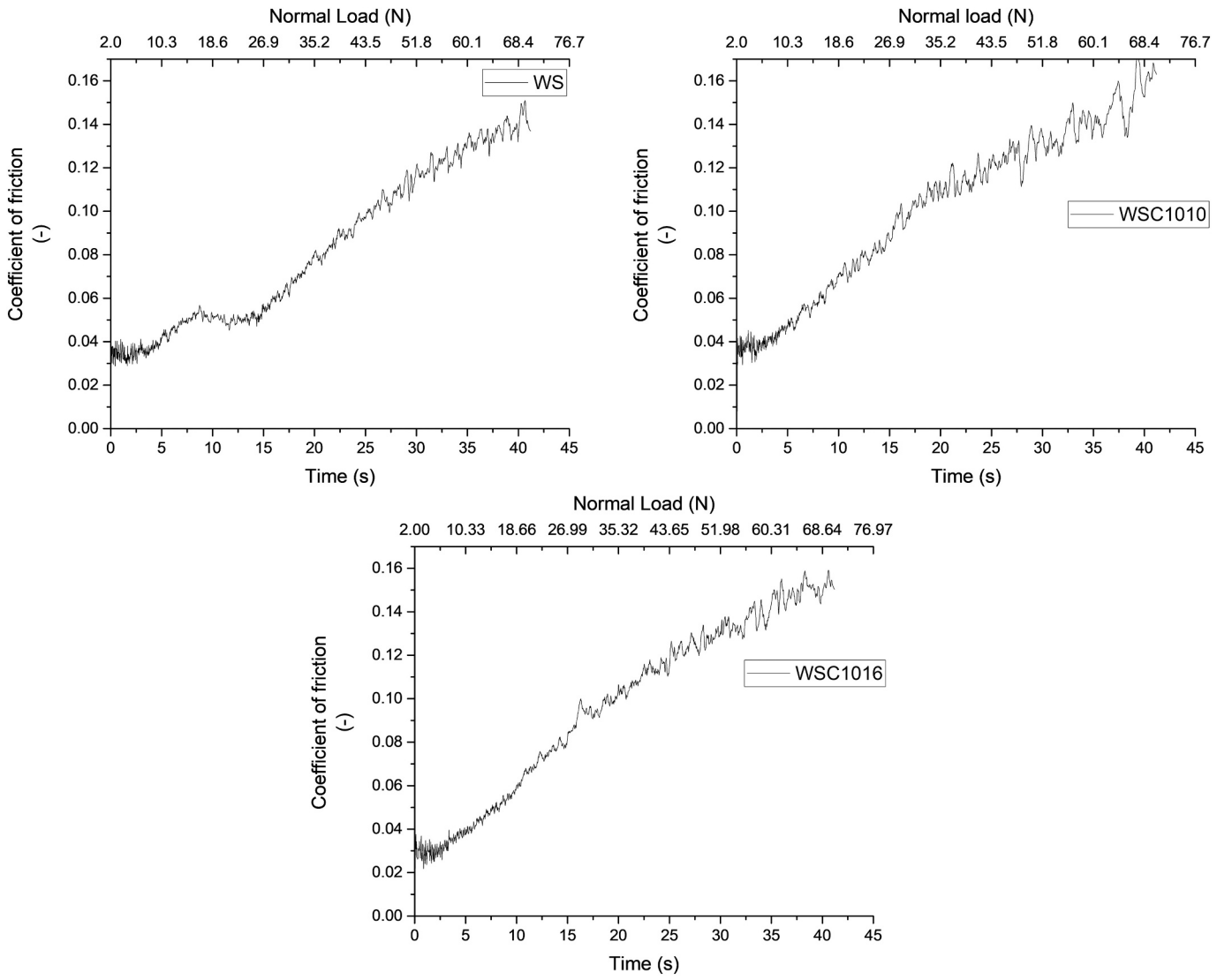

Fig. 8. Coefficient of friction measured during scratch testing.

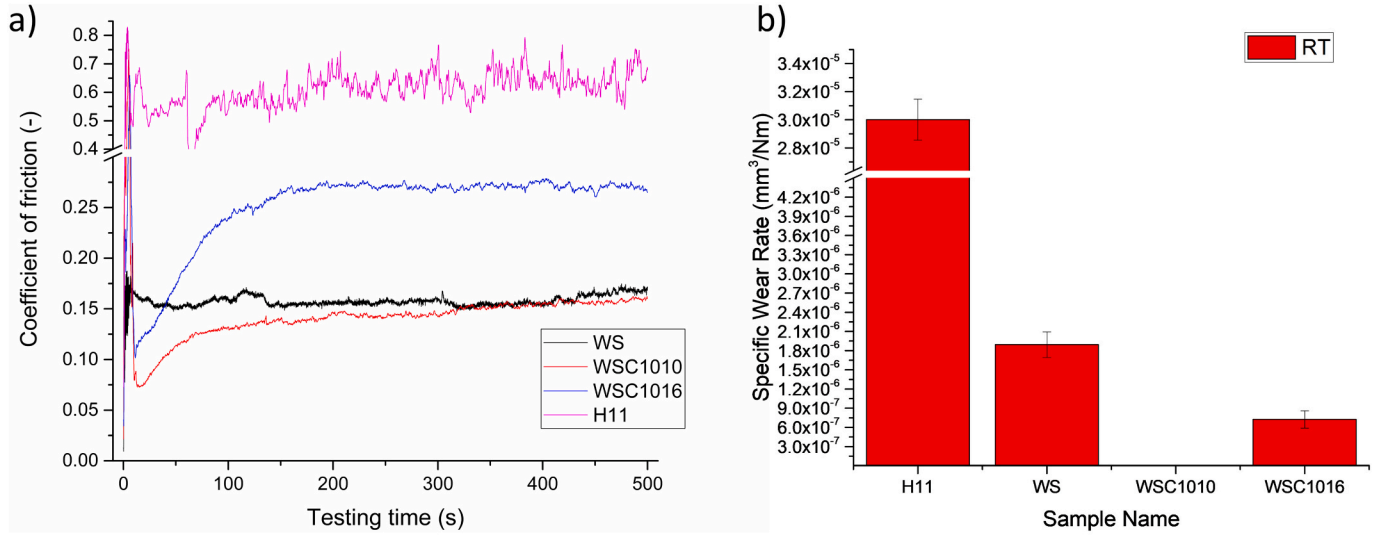

Fig. 9. Results from the tribological testing performed at RT a) COF and b) Specific wear rate.

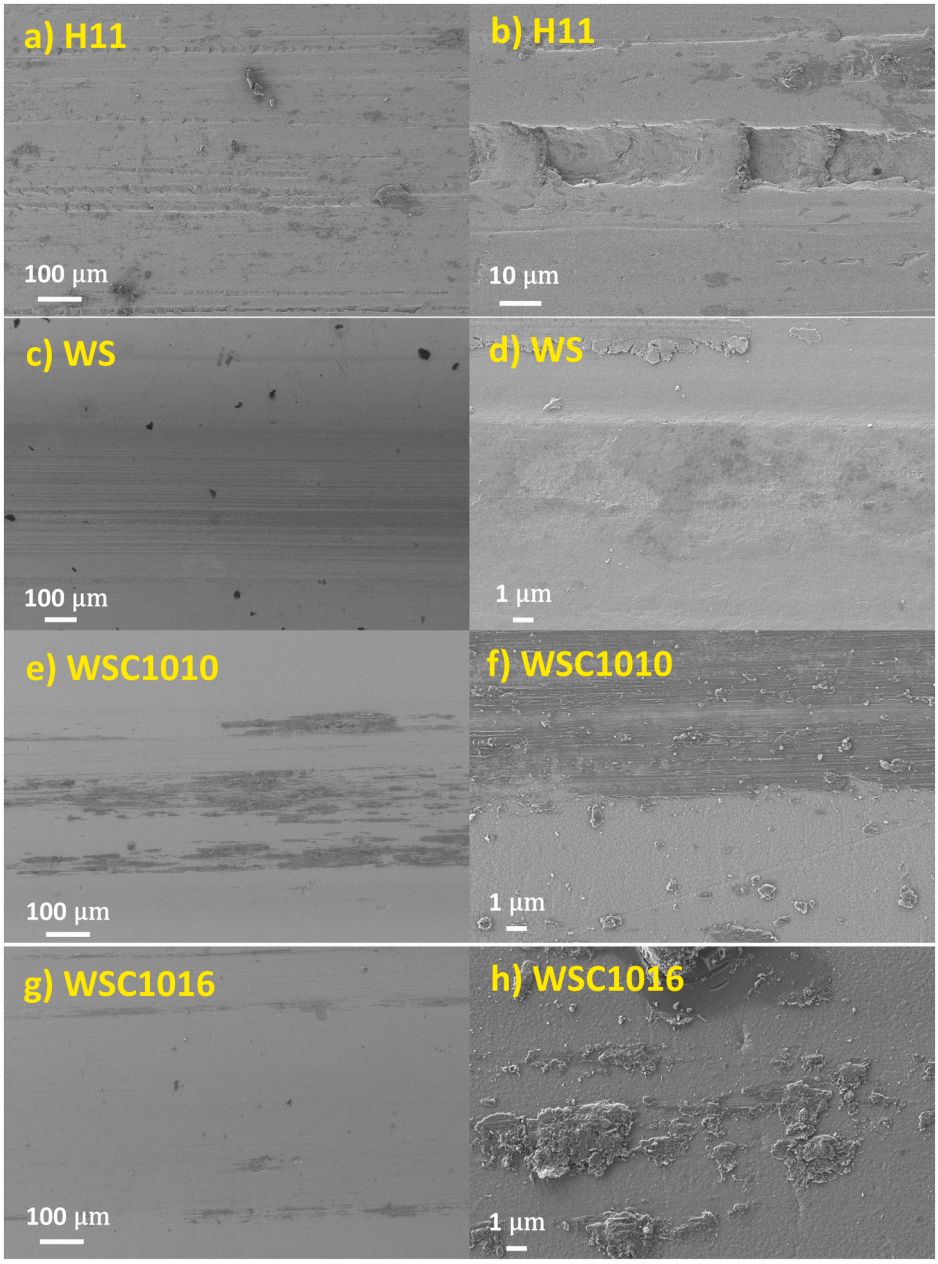

Fig. 10. SEM micrographs from the wear tracks of the disks tested at RT a,b) H11; c,d)WS; e,f) WSC1010; g,h) WSC1016.

coating deposited with the same conditions but without negative substrate bias showed a higher S/W ratio of 1.6 (see Ref. [16]). This difference is expected since, when negative substrate bias is used, the films are continuously bombarded with Ar ions, present in the proximity of the substrate due to the utilization of unbalanced magnetrons. Small amounts of carbon could also be detected in the WS coating. This is most likely contamination since during deposition of the WS coating, the graphite targets are present in the chamber. However, this amount is very small and as later shown (by Raman spectroscopy) it does not result in formation of a-C (its different as compared to when C is added intentionally in the W-S-C coatings). With the co-sputtering of graphite (500 W on each target), a carbon content of ~27 at. % and a S/W ratio of ~1.35 were achieved. Although substrate bias was not used for this case, sputtering of 3 targets simultaneously gives rise to an increase of the bombardment of the growing film causing the preferential resputtering of the volatile S atoms from the growing film [17]. The increased bombardment with Ar^+ ions in this case is due to the partial closing of the magnetic field which can significantly increase the presence of Ar^+ ions in the proximity of the substrates. These Ar^+ ions bombard the substrate due to the potential difference between the plasma and the grounded substrates. With the further increase in the power applied to the graphite targets the C content reached ~35.5 at. %. The S/W ratio increased slightly compared to the WSC1010 coating. The increased S/W ratio is very likely due to the increased number of incoming C atoms to the growing film which limit the S atoms from being resputtered. The WS coating showed a thickness of ~1.39 µm, slightly smaller compared to the WSC 1010 coating. This difference is expected as more film forming species are arriving towards the substrates for the coating containing carbon. The coating WSC 1016 has a very similar thickness in spite of the higher power applied to the graphite targets. This indicates that this coating is denser/more compact than the WSC1010 one.

The morphology of the coatings can be observed in Fig. 1. The cross-sectional imaging of the WS coating revealed a columnar growth with a porous appearance. Sputtered WS coatings often have columnar

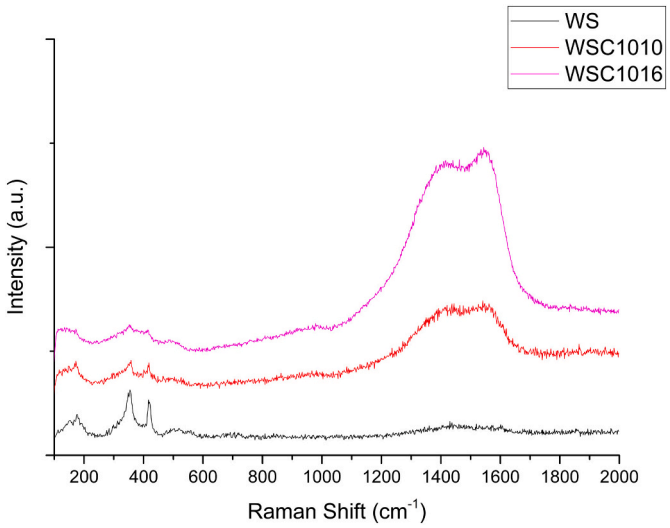

Fig. 11. Raman spectroscopy performed on the wear tracks of the disk.

morphology with a high porosity. Nevertheless, increased compactness can be observed compared to a WS coating deposited without a negative substrate bias, as it was reported in our previous publication [16]. This increase is expected due to the application of negative substrate bias since the bombardment of the film with Ar ions increases, improving the adatom mobility and restricting the columnar growth [18]. The top surface morphology was cauliflower-like, often observed for sputtered coatings. Usually, pure TMD coatings deposited without substrate bias show more porous top-surface morphologies (see for example [16,19]). This indicates that this coating has a slightly higher density than sputtered single TMD coatings. The addition of carbon (coating WSC1010) resulted in a more compact cross-sectional morphology, with reduced intercolumnar porosity, which was also reported in [20]. The coating with the highest carbon (WSC1016) content, although showing signs of columnar growth, it appears quite dense and compact. The top-surface imaging revealed quite similar cauliflower-like features. As previously mentioned, this coating with the highest compactness shows quite similar thickness compared to the WSC1010 in spite of its higher carbon content, i.e. more atoms are involved in the film growth.

The results from the XRD analysis are shown in Fig. 2. For the analysis of the WS_2 film, the only revealing the presence of WS_2 crystals, the ICDD card no 01–084-1398 was used. The strongest peak was the one stemming from the (100) planes of WS_2 ($2\theta \sim 38°$), indicating that the basal planes are oriented closely perpendicular to the substrate. The (002) WS_2 was also detected at $2\theta \sim 16°$, whose presence indicates that there are WS_2 crystals with their basal planes oriented closely parallel to the substrate. The intensities observed that are centered around $2\theta \sim 71°$ are caused by various WS_2 planes: (110) at 69°, (008) at 71° and (112) at 71.6°. Finally, the intensities observed at $2\theta \sim 81–84°$ are from the (200), (201) and (202) planes of WS_2. The carbon alloyed coatings presented amorphous-like diffractograms with a broad peak in the range of $2\theta = 35–60°$, these intensities very likely originate from the WS_2 peaks that are present there (e.g. the 100 peak) with the tail towards higher 2θ values indicating the turbostratic arrangement of the (10*L*) planes where L has values of: 1,2,3,4. Nevertheless, it is very likely that the crystals are too small to be detected using the XRD technique. It is worth mentioning that similar coatings showed TMD platelets with a thickness of up to 4 layers and length of up to ~10 nm during TEM analysis in our previous studies [10,21].

The Raman spectra obtained are shown in Fig. 3. For the WS coating the strongest peaks are at ~350–355 cm^{-1} and ~417 cm^{-1}. The former peak stems from 2 WS_2 related peaks present in this region, 2LA(M) and $E^1_{2g}(\Gamma)$. The latter peak is related to the $A_{1g}(\Gamma)$ mode [22]. The peaks observed at Raman shift values of 100–250 cm^{-1} and 450–550 cm^{-1} are weaker peaks associated with WS_2 [23]. Considering the composition, XRD and Raman analysis, the WS coatings most likely consists of crystals of WS_2 with defects in its structure (lack of S atoms). The major features observed for the WSC1010 and WSC1016 coatings are the intensities at Raman shift values in the range ~1200–1650 cm^{-1}. These intensities are related to the D and G vibration modes of carbon. The positions of the peaks are at ~1350 and 1550 cm^{-1} for the D and G, respectively. Considering the peak positions and intensities observed, the carbon phase for these coatings is of amorphous carbon (a-C) nature with sp^3 bonding type up to 20 % [24], which is typical for DC magnetron sputtered carbon films. The structure of the coatings WSC coatings is nanocomposite consisting of an a-C matrix with crystallites of WS_x embedded in it. The presence of tungsten carbides is plausible but even if they are present, they are amorphous in nature.

3.2. Thermal analysis

The results from the TGA experiments are shown in Fig. 4. For all coatings we observed a continuous mass loss with the temperature increase up to ~400° which is very likely due to evaporation of any moisture picked up by the films. This initial weight loss was higher for the more porous WS coating. The major weight loss events occurred at ~435 °C for the WS coating and ~ 480–490 °C for the carbon containing ones. These events are due to the oxidation of WS_2. The differences observed are most likely due to the presence of a-C for the carbon containing coatings which probably delays the onset of oxidation of WS_2. It should be noted that oxidation of WS_2 to WO_3 is a mass loss process. The reaction that occurs related to the oxidation of WS_2 is [25]:

$$WS_2 + 3.5\ O_2 \rightarrow WO_3 + 2SO_2$$

The a-C carbon phase is most likely oxidized to CO_2 and vented, which should result in weight loss [26,27]. Since the temperature at which there is substantial oxidation of a-C lies within the range 400–500° [27], it is highly likely that the oxidation of a-C overlapped with the oxidation of the WS_2 phase. A single mass loss event was also reported in [28], for WS_2 nanosheets that contain carbon. The weight gain observed at temperatures over 800 °C is most likely due to oxidation of the Cr interlayer. Additionally, a mass gain can also be due to further oxidation of any excess W which might not be bonded to S, please note that the S/W ratio was lower than 2 and its highly likely that there is an excess of unbonded W. Substantial oxidation of W typically occurs above 600 °C [29]. To further assess the behavior of the films at elevated temperatures we also performed in-situ GIXRD and the results from those experiments are presented in Fig. 5. The scans performed at 200 °C revealed no changes, the spectra remained the same as the ones obtained at room temperature (RT) for all the films. At 400 °C we could already observe some oxidation of the WS film. The WO_3 peaks observed were related to the monoclinic WO_3 (ICDD card no. 01–083-0950). Intensities related to the WS_2 peaks could be observed but their intensity is reduced (compare, for example, the intensity of the 002 peak at ~16°). The presence of the (100) peak of WS_2 was difficult to distinguish from the three WO_3 peaks present in the same range: (022) at ~38.8°, (−202) at ~39.1 and (202) at 39.9°. Nevertheless, it is very likely that WS_2 is still present at this temperature as intensity was also observed at $2\theta = 38°$. The XRD in this area, when the samples were further heated up to 500 °C and after cooling, revealed a narrower peak at $2\theta \sim 39°$ related to WO_3. After heating the sample at 500 °C the WS_2 was fully oxidized to WO_3. It should be noted that, for the WS sample analyzed at 400 °C, 2 well separated peaks related to WO_3 are detected at $2\theta \sim 26.9°$ (002) and $2\theta \sim 28.2°$ (200), while the scan at 500 °C revealed a single WO_3 peak at $2\theta \sim 27.8°$ (020). For the carbon alloyed films, no changes were observed at both 200 °C and 400 °C as compared to the spectrum obtained at RT, indicating that no major change occurred. The scan at 500 °C revealed the presence of WO_3, i.e. the WS_2 phase was already oxidized. These results corroborate the TGA ones, i.e. the carbon phase protects the WS_2 from oxidation. Moreover, as the films are denser, they

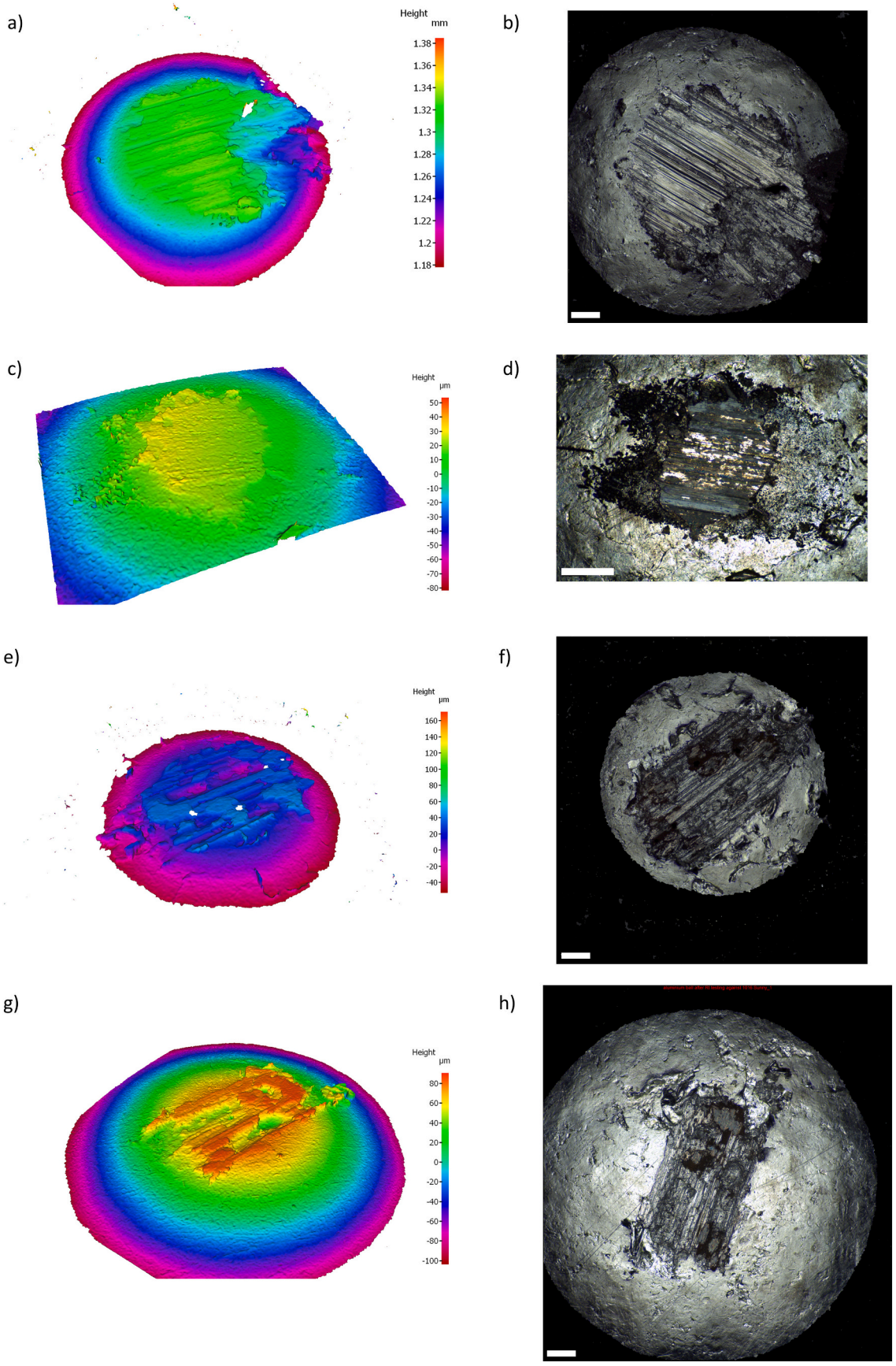

Fig. 12. 3D scans and optical micrographs of the worn alumonium balls tested at RT: a,b) Uncoated tool steel; c,d) WS; e,f) WSC1010 and g,h) WSC1016, the scale bars in the optical micrographs are 200 µm.

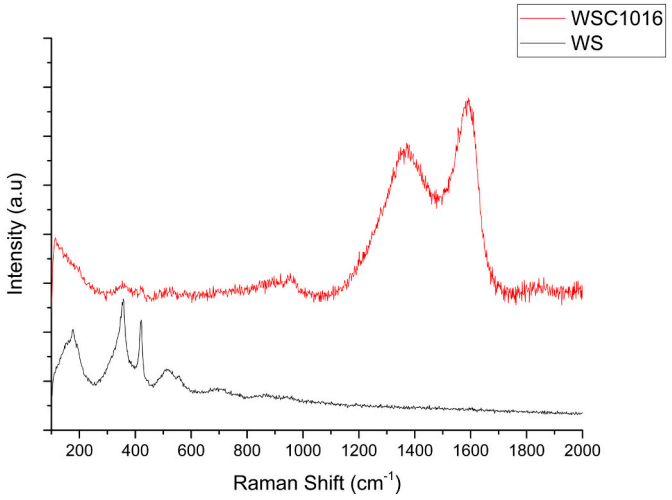

Fig. 13. Raman spectroscopy results from the wear scars of the balls tested at RT.

can prevent the inward diffusion of oxygen. Based on these results, the upper temperature limit for the usage of WS coating should be ~400 °C whereas the films containing carbon can probably be exposed to slightly higher temperatures, but not >450 °C.

3.3. Hardness and adhesion

The hardness measured as a function of the penetration depth is presented in Fig. 6. The values obtained for the WS coating are the lowest, with a value of ~2.5 GPa. The carbon alloyed coatings had a similar hardness with a value of ~5 GPa. For these coatings the hardness increase with the addition of carbon is expected since either the carbon phase is intrinsically harder than the TMD phase or the coatings are more compact. In spite of this, the pure WS coating had a higher hardness compared to other WS_x coatings where hardness down to 0.5–1 GPa was measured (see for example [16]). This increase is due to the lower S/W ratio and the increased compactness of the coating, achieved through the bombardment of the film with Ar^+ ions during deposition induced by the negative substrate bias. The reduced modulus of the coating was 48 GPa, 75 GPa and 79 GPa for the WS, WSC1010 and WSC1016 coatings, respectively.

The critical loads measured from scratch testing are shown in Table 2. The first critical load (Lc_1) is related to the first appearance of cracks. The second critical load (Lc_2) is depicted from the start of chipping at the edge of the tracks, i.e. removal of small chunks of material from the coatings. The Lc_3 load is related to the start of gross delamination or spalling of larger chunks of material from the coatings. The location of the critical loads was performed by acquiring a panoramic optical image and later measuring the distance between the start of the test to the location of the features related to the critical loads (see Fig. 7). The Lc_1 load was detected relatively early for the carbon alloyed coatings with load of 5–6 N. The unalloyed WS coating did not show any cracking and thus no Lc_1 load was detected. The WS coating had the lowest value for the Lc_2 critical load with a value of ~19 N. Both carbon alloyed coatings showed an Lc_2 value of 26–27 N. No gross delamination was detected for the current range of loads.

The location of the critical loads can also be correlated with the change of the COF during the scratch testing (Fig. 8). For the WS coating, an increase in the COF was observed at around ~15 N which can be correlated with the location of the Lc_2 load. For the WSC coatings, the COF was less stable after ~20 N, a load slightly less than the Lc_2 one. The COF showed a steady increase until the end of the scratch with no significant spikes, further corroborating the lack of gross delamination and the absence of the Lc_3 critical load. It should also be noted that the COF was relatively low with a maximum value of ~0.16 at the end of the test. The continuous increase of the COF is due to increasing plastic deformation of the substrate as the load is increased. The results indicate that the architecture, i.e. the interlayer and the gradient layer in combination with the other coating properties, gives rise to well adherent and suitable coatings for application onto tool steels that can be important for hot forming applications.

3.4. Tribology

3.4.1. Room temperature testing

The results, COF and wear rate, from the tribological testing performed at RT are shown in Fig. 9 a) and b), respectively. The uncoated steel showed a coefficient of friction of ~0.6–0.7, with an unstable behavior. The obtained values in the later stages of sliding are in agreement with the ones presented in [3]. The wear rate calculated for the steel sample was $\sim 3 \times 10^{-5}$ mm^3/Nm.

The WS and WSC 1010 coatings showed a similar steady-state COF of around 0.15. A difference between these coatings was observed in the initial stages of sliding. The WS coating did not show any significant spikes initially, while the WSC 1010 coating had a COF spike with a value up to ~0.7–0.8. The WSC 1016 coating showed similar behavior as

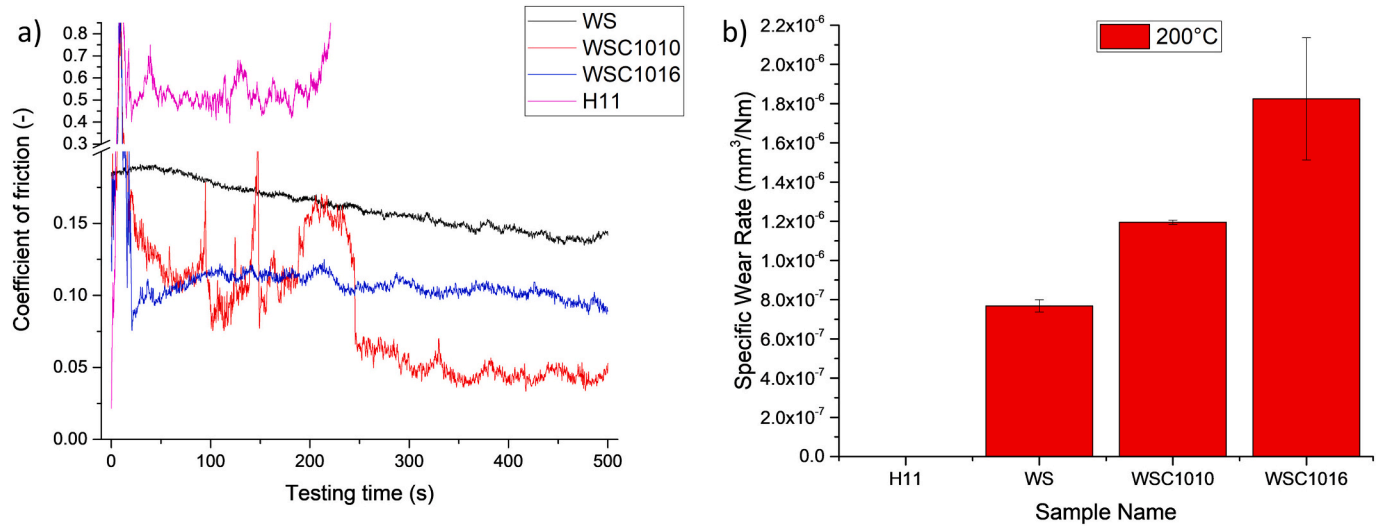

Fig. 14. Results from the tribological testing performed at 200 °C a) COF and b) Specific wear rate.

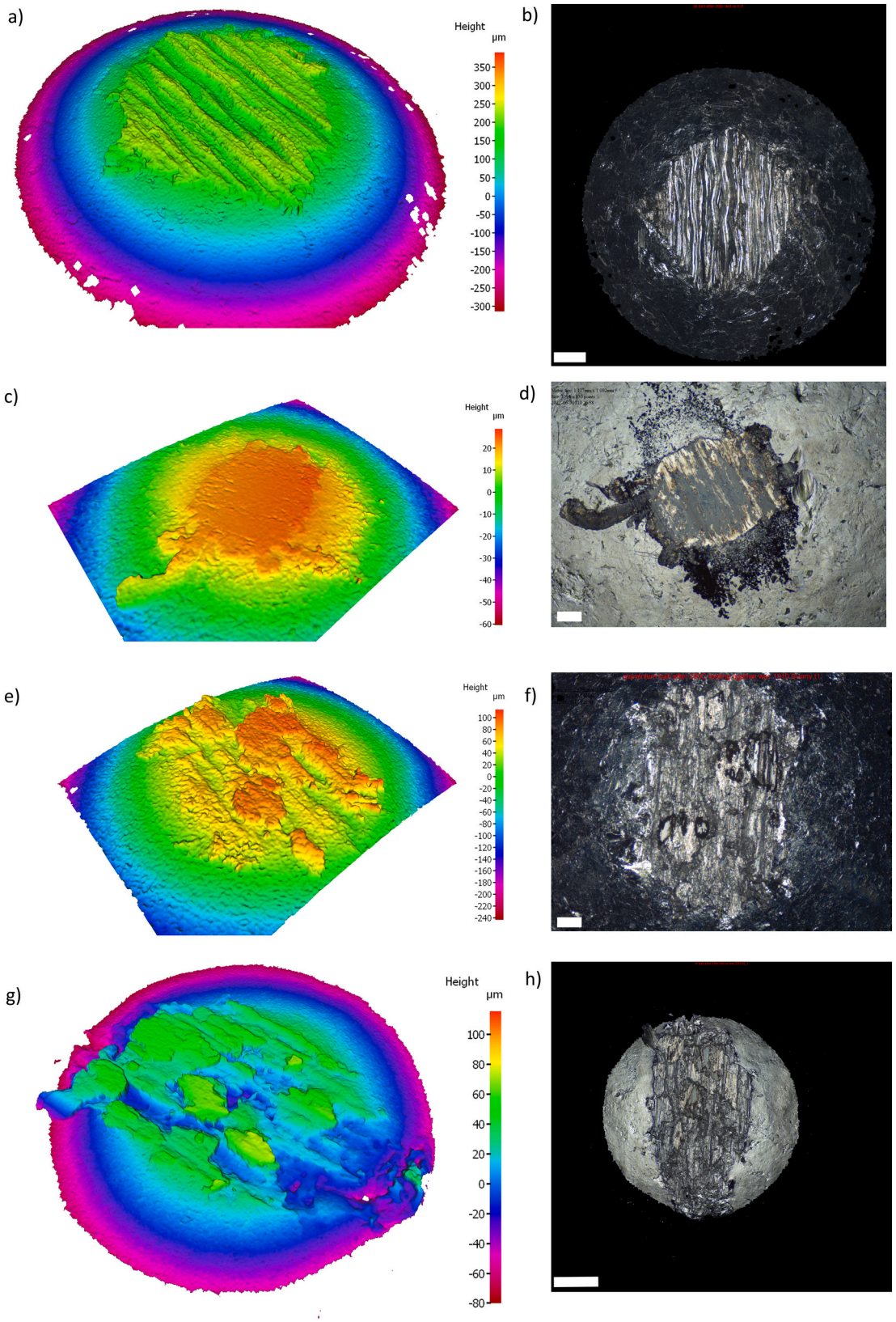

Fig. 15. 3D scans and optical micrographs of the worn aluminium balls tested at 200 °C: a,b) Uncoated tool steel; c,d) WS; e,f) WSC1010 and g,h) WSC1016, the scale bars in the optical micrographs are 200 µm.

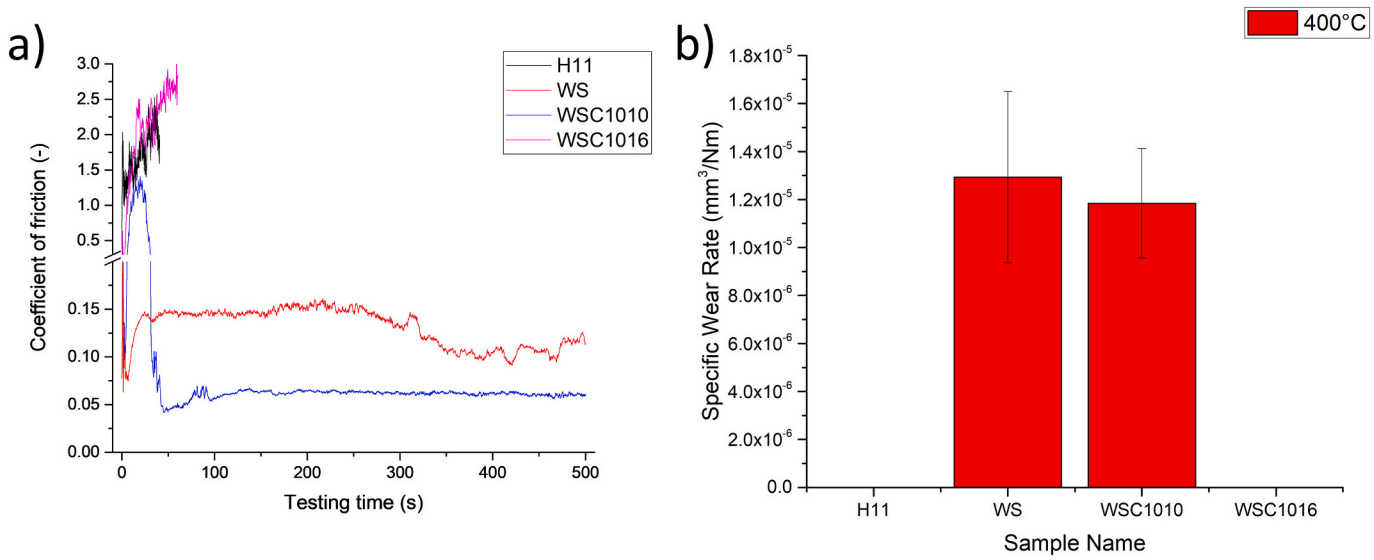

Fig. 16. Results from the tribological testing performed at 400 °C a) COF and b) Specific wear rate.

the WSC 1010 coating, with the major difference being a higher steady-state value of ~0.25. Concerning wear, the uncoated tool steel had the highest wear rate with a value of $\sim 3 \times 10^{-5}$ mm^3/Nm. The WS coating showed an order of magnitude lower wear with a value of $\sim 1.8 \times 10^{-6}$ mm^3/Nm. The wear for the WSC 1010 coating could not be assessed, the wear track showed only very minor scratches in the direction of sliding, and there was a material transfer from the aluminium counterbody which masked the wear-related features. The WSC 1016 coating had a relatively low wear with a value of $\sim 6 \times 10^{-7}$ mm^3/Nm.

The wear tracks present on the disks were analyzed using SEM and the results are presented in Fig. 10, with the subfigure on the left side showing lower magnification images and the ones on the right side, higher magnification images of the wear track. The wear track on the tool steel showed marks in the direction of sliding indicating abrasion. The depth of these features was typically ~4 μm. The abrasive wear is most probably caused by oxidized Fe and Al particles which can be abrasive. EDS performed on areas close to the abrasive marks revealed material rich in Al with a significant amount of oxygen. Similar features were observed in [3]. The wear track of the WS coating was generally smooth with the most prominent features being abrasive marks in the direction of sliding, which were not protruding through the interlayer. Raman spectroscopy was also performed (see Fig. 11) on the smooth areas within the wear track. The spectrum showed only lubricious WS_2. For the carbon alloyed coatings, the tracks revealed the presence of additional material on the wear tracks (darker features on the SEM micrographs), which were aluminium-rich, based on EDS analysis. For the WSC1010 coating, more material transfer was detected, in agreement with the aforementioned 3D analysis. The morphology of these carbon-alloyed coatings after testing appeared smoother, i.e. the cauliflower-like features were more difficult to detect. The Raman analysis performed on the smoother areas of these wear tracks uncovered the presence of more crystalline WS_2 (the peaks related to WS_2 are narrower and with higher intensity). Additionally, the D and G peaks of carbon give the impression of being more separated and the G peak is shifted to higher values, which is a sign of graphitization of the a-C.

The 3D morphology of the balls and their respective optical micrographs are presented in Fig. 12. The ball tested against the uncoated tool steel had a wear scar with a diameter of up to 600 μm with the presence of abrasion marks, all aligned in a single direction. One part of the scar was not uniform with a pit-like morphology which indicates significant removal of material. The balls tested against the carbon-alloyed coatings also presented wear, with slightly narrower wear scars and lack of larger pits, an appearance that generally indicates that the wear of the aluminium balls is reduced as compared to the one tested against the uncoated steel. A notable difference is observed for the counterbody tested against the WS coatings. It was significantly smaller than the others and presented a smoother appearance. Raman analysis was performed on the ball scars, from tests against the WS and the WSC1016 coatings (see Fig. 13). The analysis on the layers observed on the ball tested against the WS coating revealed strong WS_2 related peaks (at Raman Shift value of ~350 and ~ 417 cm^{-1}). The analysis on the layers observed at the ball tested against the WSC1016 coating revealed different features. The main thing observed were the D and G peaks related with carbon. Similarly to the layers observed on the wear track, these peaks were more separated with the G peak being shifted to higher values as compared to the spectrum observed on the as-deposited coating. Intensities related to WS_2 were observed but they were very weak. This indicates that the transferred layers have a more graphitic nature. The smallest scar for the aluminium ball tested against the WS coating is due to the faster formation of lubricious tribofilms since, in this case, during the running-in, no friction spikes were observed, as compared to the carbon-alloyed coatings. During this running-in period, it is also likely that the wear of the ball occurs, changing the contact conditions (e.g. the contact pressure). This can explain the lower friction observed for the carbon alloyed coatings compared to the WS one.

In summary, during testing at RT the wear mechanism of the tool steel is mostly abrasive wear caused by oxidized Al and Fe wear debris. The WS coating manages to quickly form a WS_2 rich tribofilm on both the disk and the ball. and thus reduce the friction with no significant friction spikes and no significant material transfer from the aluminium counterbody. The carbon-alloyed coatings manage to provide friction reduction but during the running-in process, there are friction spikes and material transfer from the aluminium counterbody. The lubricity for these coatings stems from tribofilms rich in WS_2 and graphite, with the presence of the latter being more prominent. The WS_2-based tribofilms are typically couple of nm thick and they align with the basal planes parallel (initially they have random orientation) to the direction of sliding due to the mechanical stresses and thus provide friction reduction [11].

3.4.2. *Testing at 200 °C*

The COF and the specific wear rate from testing at 200 °C are presented in Fig. 14. The ball slid against the uncoated tool steel gave rise to a COF in the range of 0.5–0.7. After approximately 200 s of sliding, the test was aborted as the COF started to increase which was accompanied by increased noise and vibration of the machine, indicating severe

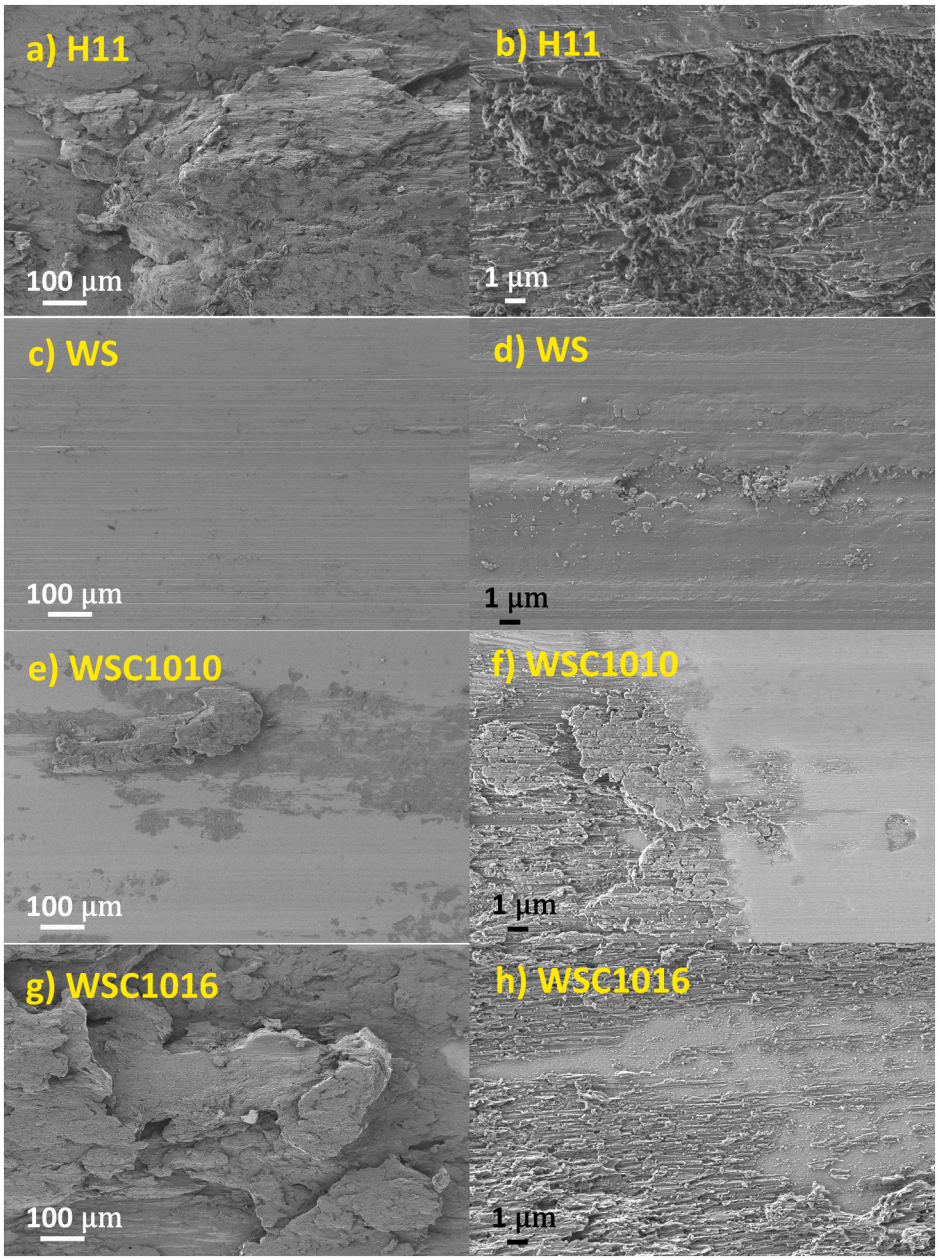

Fig. 17. SEM micrographs from the wear tracks of the disks tested at 400 °C a,b) H11; c,d)WS; e,f) WSC1010; g,h) WSC1016.

galling. The WS coating provided relatively low friction with a starting value of ~0.17–0.18 and a decreasing trend reaching a value of ~0.14–0.15 towards the end of the test. The carbon alloyed coatings showed lower COF values down to 0.05 and 0.1 for the coatings WSC1010 and WSC1016, respectively. The main difference of the carbon-alloyed coatings, in relation to the WS one, was the presence of high friction during the initial stages of sliding where COF values up to 0.7–0.8 were observed. The 3D analysis of the wear tracks revealed no wear for the uncoated tool steel, with significant material transfer from the aluminium ball. The self-lubricating coatings presented wear with the lowest values for the pure WS coating ($\sim 7 \times 10^{-7}$ mm^3/Nm). The values measured for the WSC1010 and WSC1016 coatings were slightly higher, $\sim 1 \times 10^{-6}$ and $\sim 1.8 \times 10^{-6}$ mm^3/Nm, respectively.

The topographies of the balls after testing are presented in Fig. 15. The wear scar on the ball tested against the tool steel is relatively large with a diameter of up to 1.5 mm, with elongated marks resembling scratches. The wear scar on the ball tested against the WSC1016 coating also appeared large and irregular. The smallest wear scar was observed for the WS coating. The appearance was similar to the one observed after RT testing.

The large wear scar of the ball tested against the uncoated tool steel is in agreement with the features observed on the disk, i.e. it further corroborates the material transfer from the aluminium counterbody to the disk. This mechanism is enabled by the significant thermal softening of the aluminium balls. The results are also in agreement with the ones reported in [3], where lumps of material were observed on the tool steel at a similar testing temperature. The initial instabilities observed for the carbon alloyed coatings are related to the sliding needed to form a WS_2-rich tribofilm. Since the lubrication mechanisms at this temperature are similar to the ones at 400 °C, they will be discussed in the following subsection.

3.4.3. *Testing at 400 °C*

The COF and wear results from the tribological testing at 400 °C are

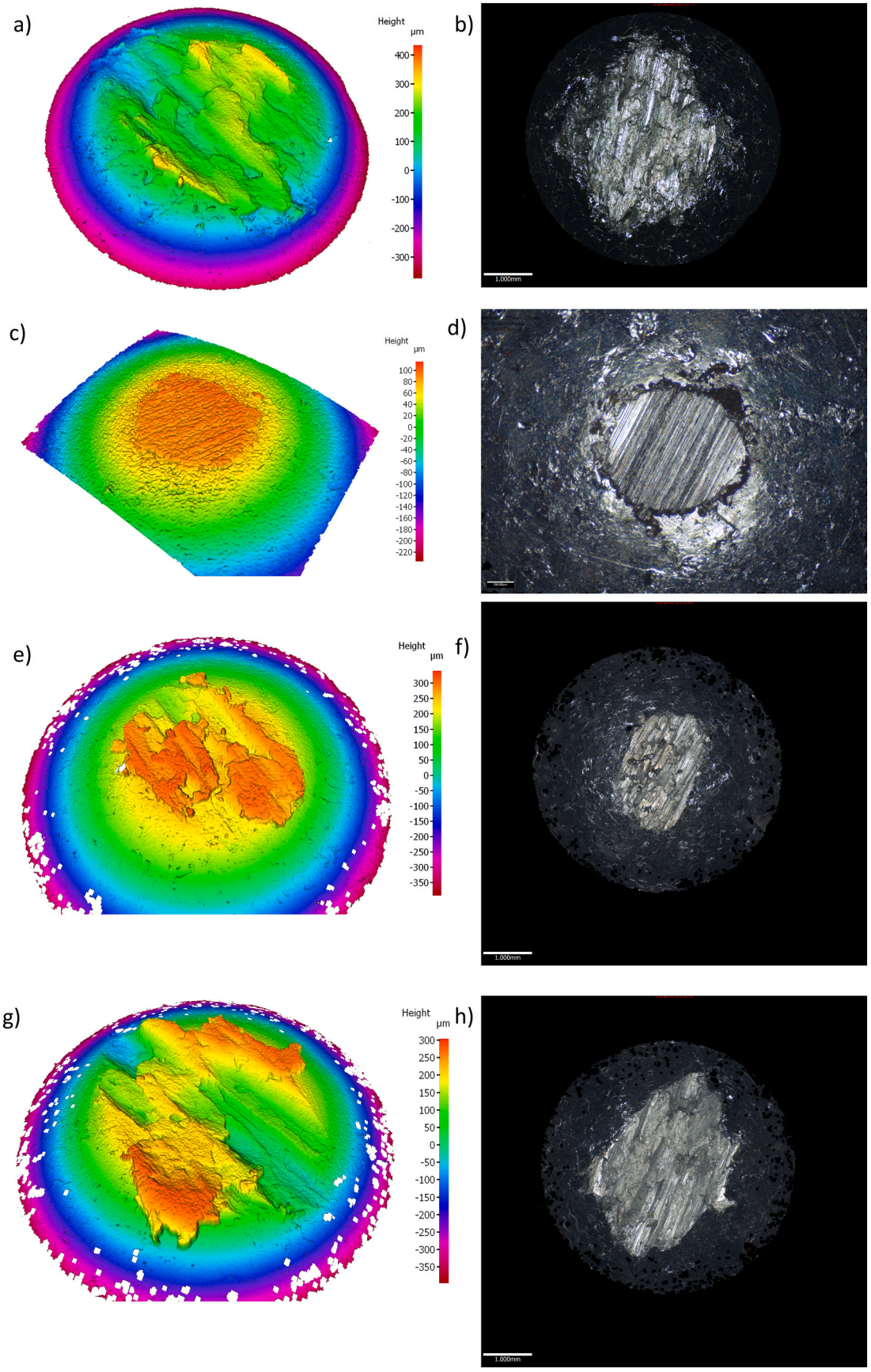

Fig. 18. 3D scans of the worn aluminium balls tested at 400 °C: a,b) Uncoated tool steel; c,d) WS; e,f) WSC1010 and g,h) WSC1016.

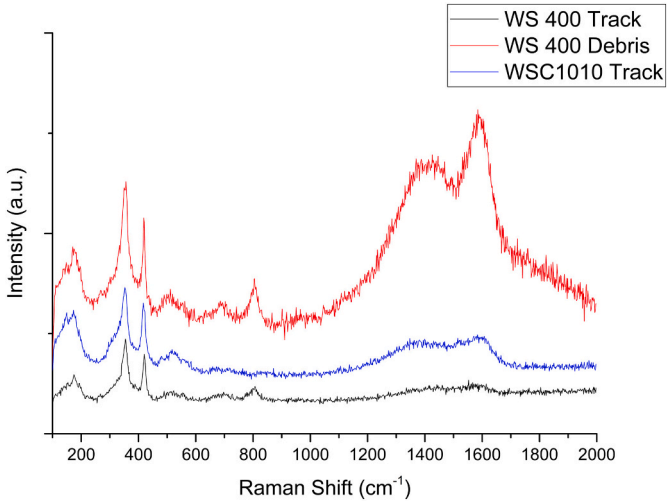

Fig. 19. Raman spectroscopy results from the wear tracks of the disks tested at 400 °C.

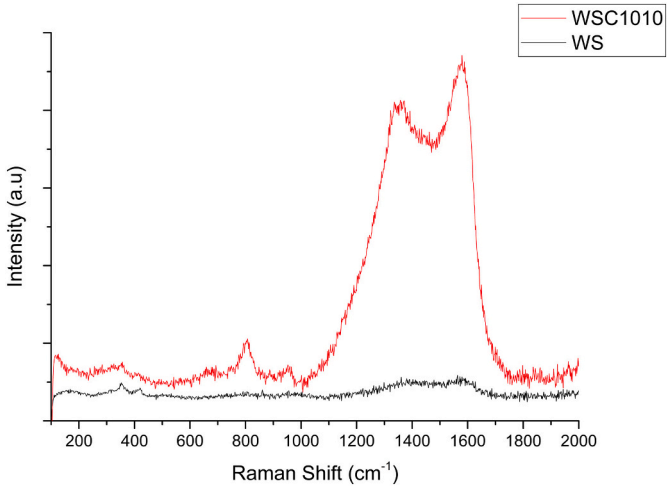

Fig. 20. Raman spectroscopy results from the wear scars of the balls tested at 400 °C.

presented in Fig. 16. Only the WS and the WSC1010 coatings managed to provide friction reduction. The uncoated tool steel and the WSC1016 coating had a continuously increasing coefficient of friction with values reaching up to 2.5, indicating severe galling. The tests were aborted in both cases. The COF for the WS coating was more stable, showing a minor dip initially to a value down to ~0.07 and then stabilizing with a value ~0.15. A drop on the COF was observed towards the end of the testing with values down to ~0.1. The WSC1010 coating showed instabilities and high COF initially and after ~50 s of sliding a drop in the COF was observed and a value of ~0.07 was maintained until the end of the experiment.

No wear could be measured for the uncoated tool steel and the WSC1016 coating as significant amount of material transfer was observed through the 3D (see supplementary information) and SEM analysis (see Fig. 17). The darker features observed in the SEM micrographs cover the whole width of the track and the EDS performed in those uncovered significant amounts of Al, confirming the hypothesis that there is significant material transfer from the aluminium counterbodies to the tool steel and the WSC1016 coating. Due to the severe galling, the sliding is aluminium against aluminium which is unfavorable as there can be severe adhesion and thus an increase in the COF. The WS and WSC1010 coatings had a wear rate of ~1–1.5 × 10^{-5} mm^3/Nm, values that are an order of magnitude higher than the ones observed during testing at 200 °C. 3D scanning (see Fig. 18) revealed significant wear on the balls tested against the uncoated steel and the WSC1016 coating. Additionally, the ball tested against WSC1010 also had an appearance which indicated higher wear compared to the one tested against the WS coating.

The Raman analysis performed (see Fig. 19) on the wear track of the WS and WSC1010 coatings, revealed the presence of WS_2. For the WSC1010 coating, the WS_2 peaks were narrower and more intense as compared to the ones in as-deposited implying crystallization of the WS_2 phase. Similar transformations were observed in our previous studies (see [6,10]). The Raman analysis performed on the wear track and on the wear debris outside of the wear track also showed intensities at a Raman shift value of ~800 cm^{-1} which are related to the presence of tungsten oxides [31]. The debris analyzed through Raman on the wear track of the WS coating showed presence of carbon which is very likely due to the minor presence of C in the coatings. It should be also noted that this spectrum showed strong fluorescence and the D and G peaks of carbon might be exaggerated due to the background removal. An attempt was also made to perform Raman on the Al balls after testing (see Fig. 20). In the case of the one sliding against the WS coating, the analysis was performed in areas that appeared darker under the optical microscope and resembled layers transferred from the disk. Intensities related to WS_2 could be identified (peaks at ~350 and 417 cm^{-1}), coupled with minor intensities related to graphitic carbon. Obtaining Raman spectrum from the ball tested against the WSC1010 coating was more difficult as the scar was more irregular, and it was difficult to identify features that appeared different than the aluminium. Nevertheless, analysis was performed in some areas where features resembling layers transferred from the coating were identified. It revealed strong presence of graphitic carbon with very minor intensities that can related to presence of WS_2 and a peak at 800 cm^{-1} which is related to tungsten oxides. For the ball tested against the WSC1016 ball, we could not observe any features other than what appeared to be a significantly worn ball with irregular morphology.

Regarding the COF, the high values observed for the uncoated steel/WSC1016-aluminium tribopairs are in agreement with the one measured in [3,4], i.e. values up to 2 were observed for a similar tool steel-aluminium tribopair tested at similar temperatures. It is interesting to note that the WSC1016 coating could not provide lubrication. This is most likely because tribofilms could not be established. The aluminium ball softens significantly at these temperatures and preferentially wears. The WSC1016 coating has the highest amount of carbon content and was the hardest one. Therefore, it is expected to need extra time to establish the WS_2-rich tribofilm. Nevertheless, after the severe galling the formation of the tribofilm is prevented and no lubricity is found for this coating. The ability of the coating WSC1010 to provide lubrication can be correlated with the higher abundance of W and S in the coating which helps the formation of the tribofilm. Finally, unalloyed WS coating can provide the best control for the COF in these testing conditions. The formation of the WS_2-rich tribofilms occurs rather fast and no strong fluctuations were observed during the whole duration of the test.

The low COF can mostly be attributed to the presence of WS_2 on the sliding interface as the TMDs are very good lubricants in environments lacking humidity. The presence of graphite through graphitization of the carbon phase can further provide some levels of lubrication but it must be noted that non-hydrogenated DLCs usually cannot provide significant levels of lubrication through graphitization in environments lacking humidity (see for example [1,30]). The graphite layers need to be passivated by water vapour or hydrogen in order to prevent strong interaction between the carbon atoms which hinders its lubricity. If we compare the Raman spectra obtained in an as-deposited state and the one obtained from the wear track of the coatings WSC1010, we can observe that the WS_2-related intensities are significantly increased as compared to the carbon/graphite-related ones, further supporting the

hypothesis that the friction reduction is due to presence of WS_2 on the sliding interface. The higher wear observed for the carbon alloyed coatings can be correlated with the initial instabilities observed, i.e. an amount of material needs to be "consumed" in order to form the tribofilms, and, considering the trends observed, this amount can be correlated with the content of W and S present in the coating. The overall increase of the wear for the WS and WSC1010 coatings can be associated with accelerated oxidation of the WS_2 tribofilms due to the higher testing temperature and the additional frictional heating occurring. This hypothesis is supported by the fact that Raman intensities related to tungsten oxides were observed on the wear track and the wear debris outside of the wear track.

In summary, the tribological behavior during testing at 400 °C appears to be a response to two processes that can occur in the contact. The first one being the formation of WS_2-rich tribofilms through mild wear/reorientation of the TMD crystals of the coating, resulting in reduction in friction. The second process is significant wear of the aluminium counterbody, resulting in material (aluminium) transfer to the coating and prevention of the formation of WS_2-based tribofilm and continuously increasing friction due to the severe adhesion of the aluminium-aluminium contact coupled with the accelerated wear of the aluminium which is significantly softened at this temperature.

4. Conclusions

In this study, WS_x and WS_x + C (2 different carbon contents) were synthesized by magnetron sputtering and their potential for reducing friction in contact with aluminium was assessed. The morphological analysis revealed dense morphologies for the carbon alloyed coatings, with a columnar growth for the pure WS coating. X-ray diffraction revealed the presence of crystalline WS_2 for the pure WS coating, while the coatings with additions of carbon showed amorphous-like spectra. The thermal analysis (TGA and in-situ high-temperature X-ray diffraction) indicated that the carbon alloyed coatings had slightly better resistance to oxidation (maximum temperature of ~480–490 °C) as compared to the pure WS coatings which showed signs of oxidation even at a temperature of 400 °C. The coatings were well adherent to the steel substrates as revealed by scratch testing with Lc_2 values of ~20 to 30 N and no delamination or gross spallation with loads up to 70 N. During RT tribological testing, all coatings managed to reduce friction with the best results for the pure WS and the lower carbon content coatings. The testing at 200 °C revealed lower friction for the carbon alloyed coating than the pure WS one, but the friction appeared less stable.

Based on the results, for sliding contacts of tool steel against aluminium at temperatures between 25 and 400 °C, the best candidate coating seems to be the WS one, despite a lower maximum operating temperature. In fact, this coating is less resistant to oxidation as compared to the carbon-alloyed ones. However, the coating with a low amount of carbon (~25 at. %) could also be interesting for these applications since its lower performance was due to a higher difficulty in the formation of the lubricious tribolayer. In spite of presenting a lower CoF than the pure WS, a higher amount of material was needed for the formation of the tribolayer which was reflected in a higher wear rate. For longer tests, this drawback can be recovered which will be the subject of future work where the optimization of the carbon content will be also studied. The goal would be a fast formation of the lubricious WS_2 layers without losing the oxidation resistance.

CRediT authorship contribution statement

Todor Vuchkov: Writing – original draft, Methodology, Investigation, Formal analysis, Data curation, Conceptualization. **Saniat Jahan Sunny:** Writing – review & editing, Investigation, Data curation. **Albano Cavaleiro:** Writing – review & editing, Supervision, Funding acquisition, Formal analysis, Conceptualization.

Declaration of competing interest

The authors declare that they have no known competing financial interests or personal relationships that could have appeared to influence the work reported in this paper.

Data availability

Data will be made available on request.

Acknowledgements

This work is sponsored by FEDER and by National funds through FCT-Fundação para a Ciência e a Tecnologia under the projects: CEMMPRE ref. "UIDB/00285/2020" and ARISE ref. "LA/P/0112/2020". This work was supported by the project Sim2Adapt (reference 2022.02370.PTDC, doi: 10.54499/2022.08459.PTDC), funded by Portuguese Foundation for Science and Technology. This research was also funded by PRR - Recovery and Resilience Plan and by the Next Generation EU Funds, following NOTICE N.° 02/C05-i01/2022, Component 5 – Capitalization and Business Innovation - Mobilizing Agendas for Business Innovation under the AM2R project "Mobilizing Agenda for business innovation in the Two Wheels sector" (reference: 7253).

Appendix A. Supplementary data

Supplementary data to this article can be found online at https://doi.org/10.1016/j.surfcoat.2024.130750.

References

[1] E. Konca, Y.T. Cheng, A.M. Weiner, J.M. Dasch, A.T. Alpas, Elevated temperature tribological behavior of non-hydrogenated diamond-like carbon coatings against 319 aluminum alloy, Surf. Coat. Technol. 200 (2006) 3996–4005, https://doi.org/10.1016/j.surfcoat.2005.02.202.

[2] A.A. Gharam, M.J. Lukitsch, M.P. Balogh, A.T. Alpas, High temperature tribological behaviour of carbon based (B4C and DLC) coatings in sliding contact with aluminum, Thin Solid Films 519 (2010) 1611–1617, https://doi.org/10.1016/j.tsf.2010.07.074.

[3] J. Pujante, L. Pelcastre, M. Vilaseca, D. Casellas, B. Prakash, Investigations into wear and galling mechanism of aluminium alloy-tool steel tribopair at different temperatures, Wear 308 (2013) 193–198, https://doi.org/10.1016/j.wear.2013.06.015.

[4] H. Torres, T. Caykara, H. Rojacz, B. Prakash, M. Rodríguez Ripoll, The tribology of ag/MoS2-based self-lubricating laser claddings for high temperature forming of aluminium alloys, Wear 442–443 (2020) 203110, https://doi.org/10.1016/j.wear.2019.203110.

[5] H. Torres, B. Podgornik, M. Jovičević-Klug, M. Rodríguez Ripoll, Compatibility of graphite, hBN and graphene with self-lubricating coatings and tool steel for high temperature aluminium forming, Wear 490–491 (2022) 204187, https://doi.org/10.1016/j.wear.2021.204187.

[6] T. Vuchkov, M. Evaristo, T. Bin Yaqub, T. Polcar, A. Cavaleiro, Synthesis, microstructure and mechanical properties of W–S–C self-lubricant thin films deposited by magnetron sputtering, Tribol. Int. 150 (2020) 106363. doi:https://doi.org/10.1016/j.triboint.2020.106363.

[7] S. Prasad, J. Zabinski, Super slippery solids, Nature 387 (1997) 761, https://doi.org/10.1038/42820.

[8] H. Torres, M. Rodríguez Ripoll, B. Prakash, Tribological behaviour of self-lubricating materials at high temperatures, Int. Mater. Rev. 63 (2018) 309–340, https://doi.org/10.1080/09506608.2017.1410944.

[9] T. Vuchkov, T. Bin Yaqub, M. Evaristo, A. Cavaleiro, Synthesis, microstructural and mechanical properties of self-lubricating Mo-Se-C coatings deposited by closed-field unbalanced magnetron sputtering, Surf. Coat. Technol. 394 (2020) 125889, https://doi.org/10.1016/j.surfcoat.2020.125889.

[10] T. Vuchkov, M. Evaristo, T. Bin Yaqub, A. Cavaleiro, The effect of substrate location on the composition, microstructure and mechano-tribological properties of W-S-C coatings deposited by magnetron sputtering, Surf. Coat. Technol. 386 (2020) 125481, https://doi.org/10.1016/j.surfcoat.2020.125481.

[11] T. Bin Yaqub, T. Vuchkov, S. Bruyère, J.-F. Pierson, A. Cavaleiro, A revised interpretation of the mechanisms governing low friction tribolayer formation in alloyed-TMD self-lubricating coatings, Appl. Surf. Sci. 571 (2022) 151302, https://doi.org/10.1016/j.apsusc.2021.151302.

[12] T. Vuchkov, V. Leviandhika, A. Cavaleiro, On the tribological performance of magnetron sputtered W-S-C coatings with conventional and graded composition, Surf. Coat. Technol. 449 (2022) 128929, https://doi.org/10.1016/j.surfcoat.2022.128929.

[13] W.C. Oliver, G.M. Pharr, An improved technique for determining hardness and elastic modulus using load and displacement sensing indentation experiments, J. Mater. Res. 7 (1992) 1564–1583, https://doi.org/10.1557/JMR.1992.1564.
[14] ISO - ISO 14577-4:2016 - Metallic materials — Instrumented indentation test for hardness and materials parameters — Part 4: Test method for metallic and non-metallic coatings, (n.d.).
[15] ISO, ISO 20502:2005 - Fine ceramics (advanced ceramics, advanced technical ceramics) — Determination of adhesion of ceramic coatings by scratch testing, 2016.
[16] T. Vuchkov, M. Evaristo, A. Carvalho, A. Cavaleiro, On the tribological performance of laser-treated self-lubricating thin films in contact with rubber, Tribol. Int. 174 (2022) 107758, https://doi.org/10.1016/j.triboint.2022.107758.
[17] J.R. Lince, D.J. Carre, P.D. Fleischauer, Effects of argon-ion bombardment on the basal plane surface of molybdenum disulfide, Langmuir 2 (1986) 805–808, https://doi.org/10.1021/la00072a026.
[18] I. Petrov, P.B. Barna, L. Hultman, J.E. Greene, Microstructural evolution during film growth, J. Vac. Sci. Technol. A Vacuum, Surfaces, Film. 21 (2003) S117–S128, https://doi.org/10.1116/1.1601610.
[19] T. Vuchkov, T. Bin Yaqub, M. Evaristo, A. Cavaleiro, Synthesis, microstructural and mechanical properties of self-lubricating Mo-Se-C coatings deposited by closed-field unbalanced magnetron sputtering, Surf. Coat. Technol. 394 (2020) 125889, https://doi.org/10.1016/j.surfcoat.2020.125889.
[20] H. Cao, J.T.M. De Hosson, Y. Pei, Effect of carbon concentration and argon flow rate on the microstructure and triboperformance of magnetron sputtered WS2/a-C coatings, Surf. Coat. Technol. 332 (2017) 142–152, https://doi.org/10.1016/J.SURFCOAT.2017.06.087.
[21] T. Bin Yaqub, T. Vuchkov, P. Sanguino, T. Polcar, A. Cavaleiro, Comparative study of DC and RF sputtered MoSe2 coatings containing carbon—an approach to optimize stoichiometry, microstructure, crystallinity and hardness, Coatings 10 (2020) 133, https://doi.org/10.3390/coatings10020133.
[22] A. Berkdemir, H.R. Gutiérrez, A.R. Botello-Méndez, N. Perea-López, A.L. Elías, C.-I. Chia, B. Wang, V.H. Crespi, F. López-Urías, J.-C. Charlier, H. Terrones, M. Terrones, Identification of individual and few layers of WS2 using Raman spectroscopy, Sci. Rep. 3 (2013) 1755, https://doi.org/10.1038/srep01755.
[23] J.-W. Chung, A. Adib, Z.R. Dai, K. Adib, F.S. Ohuchi, Raman scattering and high resolution electron microscopy studies of metal-organic chemical vapor deposition-tungsten disulfide thin films, Thin Solid Films 335 (1998) 106–111, https://doi.org/10.1016/S0040-6090(98)00954-7.
[24] A.C. Ferrari, J. Robertson, Interpretation of Raman spectra of disordered and amorphous carbon, Phys. Rev. B 61 (2000) 14095–14107, https://doi.org/10.1103/PhysRevB.61.14095.
[25] C. Schuffenhauer, G. Wildermuth, J. Felsche, R. Tenne, How stable are inorganic fullerene-like particles? Thermal analysis (STA) of inorganic fullerene-like NbS2, MoS2, and WS2 in oxidizing and inert atmospheres in comparison with the bulk material, Phys. Chem. Chem. Phys. 6 (2004) 3991–4002, https://doi.org/10.1039/B401048E.
[26] M.-C. Chiu, W.-P. Hsieh, W.-Y. Ho, D.-Y. Wang, F.-S. Shieu, Thermal stability of Cr-doped diamond-like carbon films synthesized by cathodic arc evaporation, Thin Solid Films 476 (2005) 258–263, https://doi.org/10.1016/j.tsf.2004.09.029.
[27] W.-J. Wu, M.-H. Hon, Thermal stability of diamond-like carbon films with added silicon, Surf. Coat. Technol. 111 (1999) 134–140, https://doi.org/10.1016/S0257-8972(98)00719-1.
[28] H.K. Adigilli, B. Padya, L. Venkatesh, V.S.K. Chakravadhanula, A.K. Pandey, J. Joardar, Oxidation of 2D-WS2 nanosheets for generation of 2D-WS2/WO3 heterostructure and 2D and nanospherical WO3, Phys. Chem. Chem. Phys. 21 (2019) 25139–25147, https://doi.org/10.1039/C9CP01890E.
[29] V.E. Ivanov, High temperature oxidation protection of tungsten, National Aeronautics and Space Administration 583 (1969).
[30] T. Krumpiegl, H. Meerkamm, W. Fruth, C. Schaufler, G. Erkens, H. Böhner, Amorphous carbon coatings and their tribological behaviour at high temperatures and in high vacuum, in: Surf. Coatings Technol., 1999: pp. 555–560. doi: https://doi.org/10.1016/S0257-8972(99)00435-1.
[31] J. Chen, D. Lu, W. Zhang, F. Xie, J. Zhou, L. Gong, X. Liu, S. Deng, N. Xu, Synthesis and Raman spectroscopic study of W20O58 nanowires, J. Phys. D. Appl. Phys. 41 (2008) 115305.